Available online at www.sciencedirect.com
ScienceDirect
Journal of Sound and Vibration 319 (2009) 15–40
JOURNAL OF SOUND AND VIBRATION
www.elsevier.com/locate/jsvi

Optimal vibration control of smart fiber reinforced composite shell structures using improved genetic algorithm

Tarapada Roy, Debabrata Chakraborty*

Department of Mechanical Engineering, Indian Institute of Technology Guwahati, Guwahati 781039, India

Received 18 February 2008; received in revised form 16 May 2008; accepted 24 May 2008
Handling Editor: J. Lam
Available online 17 July 2008

Abstract

In the present article, an improved genetic algorithm (GA) based optimal vibration control of smart fiber reinforced polymer (FRP) composite shell structures has been presented. Layered shell finite elements have been formulated and the formulation has been validated for coupled electromechanical analysis of curved smart FRP composite structures having piezoelectric sensors and actuators patches. An integer-coded GA-based open-loop procedure has been used for optimal placement of actuators for maximizing controllability index and a real-coded GA-based linear quadratic regulator (LQR) control scheme has been implemented for optimal control of the smart shell structures in order to maximize the closed-loop damping ratio while keeping actuators voltages within the limit of breakdown voltage. Results obtained from the present work show that this combined GA-based optimal actuators placement and GA-based LQR control scheme is far superior to conventional active vibration control using LQR schemes and simple placement of actuators reported in literatures. Results also show that the present improved GA-based combined optimal placement and LQR control scheme not only leads to increased closed-loop damping ratio but also shows a drastic reduction in input/actuation voltage compared to the already published results.

1. Introduction

Active vibration control in distributed structures is of practical interest because of the demanding requirement for guaranteed performance. This is particularly important in lightweight structures as they generally have low internal damping and susceptible to large vibration with long decay time. Design process of such a system encompasses three main phases such as structural design, optimal placement of sensors and actuators and controller design. Integration of piezoelectric sensors and actuators to advanced composites using appropriate control technology led to light weight structure which are capable of self-monitoring and self-controlling. However, there is still a need for improved sensing and actuation both at the material and systems level. An important issue associated with such smart structures is the optimal placement of sensors and actuators to achieve most effective actuation. Since the location of actuators decide the input voltage

*Corresponding author. Tel.: +91 361 2582666; fax: +91 361 2690762.
E-mail address: chakra@iitg.ernet.in (D. Chakraborty).

0022-460X/$ - see front matter © 2008 Elsevier Ltd. All rights reserved.
doi:10.1016/j.jsv.2008.05.037

requirement for desired damping effect, it is also important to have an optimization scheme for determining the optimal placement of actuators. Two basic approaches namely open-loop approach and closed-loop approach are normally used for optimal placement of sensors and actuators. The open-loop procedure significantly simplifies the problem as the selection is performed independently of any control law. Design of an optimal controller avoids the tasks of arbitrarily finding the gain of the controller to meet the design objectives and overcomes the problems of instability and actuator saturation. At present, the linear quadratic regulator (LQR) control approach has been found to be effective in vibration control with appropriate weighting matrices, which gives optimal control gain by minimizing the performance index. The weighting matrices $[Q]$ and $[R]$ are the most important components in LQR optimization. The combinations of $[Q]$ and $[R]$ matrices greatly affect the output performance and input cost of the system and hence an optimal selection of these weighting matrices is of significant importance from the control point of view. Commonly, trial and error method is used to arrive at these matrices to achieve optimal gain. In the recent years, genetic algorithm (GA) has been extensively used for optimization of engineering problems due to its many advantages over classical optimization techniques such as it is blind search method and highly parallel. The choice of genetic coding is also very important depending on the continuous or discrete search space. For more discrete space such as actuators/sensors positioning in the smart structures integer-coded GA is more efficient than binary-coded GA because the latter requires increased string length and computational time especially in the large-scale structures where possible combination sensors/actuators are large. Important works published in this direction of active vibration control as well as application of GAs for solving engineering problems are presented in the following paragraph.

Bailey and Hubbard [1] used the angular velocity at the tip of an isotropic cantilever beam with constant-gain and constant-amplitude negative velocity algorithms and experimentally achieved the vibration control. Crawley and Luis [2] applied the mechanism of actuation strain concept for simple elastic smart beams. Lee [3] described theory of laminated piezoelectric plates with governing equations and reciprocal relations for the design of distributed sensors/actuators. Tzou and Tseng [4] studied the structural identification and control of plate model with distributed piezoelectric sensors/actuators and proposed thin piezoelectric hexahedron finite element with three internal degrees of freedom for the analysis. Chen et al. [5] proposed a new three-dimensional thin-shell structure containing an integrated distributed piezoelectric sensor and actuator. Haramoto et al. [6] presented the optimal placement of two pairs of sensors and actuators in order to maximize the H_2 norm of the closed-loop system for a simply supported beam using quasi-Newton method. Wang and Wang [7] proposed a controllability index for optimal locations and size of piezoelectric actuators, which was related to the amount of input energy required in the control design and reported that higher the controllability index, the smaller would be the electrical potential required for active control. Zhang and Kirpitchenko [8] performed vibration suppression analysis of a cantilever beam with piezoelectric sensors/actuators subjected to an exciting force. They considered two sets of surface bonded piezoelectric patches with three locations of patches and experimentally showed that the damping of combined beam-piezoelectric patches system increased by 8–10 times in comparison to that of mechanical system. Bhattacharya et al. [9] used LQR strategy for vibration suppression of spherical shells made of laminated composites by trial and error selection of $[Q]$ and $[R]$ matrices. Saravanos et al. [10] studied the impact response of adaptive piezoelectric laminated plates. They developed a semi-analytical model for predicting the electromechanical impact response of piezoelectric plates having distributed actuator and sensor layers. Ang et al. [11] proposed the use of total weighted energy method to select the weighting matrices. Narayanan and Balamurugan [12] presented finite element modeling of laminated structures with distributed piezoelectric sensor and actuator layers and applied LQR control scheme to control the displacement by trial and error selection of $[Q]$ and $[R]$ matrices. Christensen and Santos [13] proposed an active control system to control blade as well as rotor vibrations in a couple rotor blade system using tip mass actuators and sensors. They analyzed only four different actuators configurations to obtain optimal actuators placement based on the controllability index and the sensors were assumed to be mounted at the same positions to measure the position of the hub or the defection of blades. After placement of sensors and actuators, they applied LQR control scheme for vibration control of couple rotor blade system by trial and error selection of $[Q]$ and $[R]$ matrices.

In the recent years, GA has been extensively applied as a tool for optimization of engineering problems in the field of active vibration control. Han and Lee [14] applied binary-coded GA to find locations of two

piezoelectric sensors and actuators in a cantilever composite plate based on the open-loop performance. Sadri et al. [15] used Gray-coded GA to find the eight coordinates of two piezoelectric actuators in a simply supported plate based on the open-loop performance. However, this type of Gray-coded GA leads to increased string length. Abdullah et al. [16] used GA to simultaneously place collocated sensor/actuator pairs in multi-story building while using output feedback as the control law in terms of minimizing the quadratic performance i.e. weighted energy of the system. They found optimal gain using Davidon–Fletcher–Powell gradient-based optimization algorithm by choosing $[Q]$ and $[R]$ matrices using trial and error and concluded that the decision variables in this optimization problem were greatly dependent on the selection of weighting matrices $[Q]$ and $[R]$. They also used binary-coded GA with the length of the gene string as the number of floors in multi-storey building, which led to large number of function evaluations and large number of generations to reach near optimal solution. Robandi et al. [17] presented the use of GA for optimal feedback control in multi-machine power system. Deb and Gulati [18] presented simulated binary crossover (SBX) and parameter based mutation operator to be used for effective creation of children solutions from parent solutions. Guo et al. [19] presented a sensor placement optimization performance index based on the damage detection in the two-dimensional truss structures using binary-coded GA. Li et al. [20] proposed two-level genetic algorithms (TLGA) for optimal placement of active tendon actuators in multi-story building by minimizing the maximum top floor displacement. This TLGA may be feasible for this type of optimization problem. For active vibration control of large-scale structures with complete electromechanical analysis considering PZT sensors/actuators, this TLGA will not be computationally feasible because there are more possible actuators locations. Yang et al. [21] presented a simultaneous optimization method considering several design variables such as placement of collocated piezoelectric sensors/actuators and size of sensor/actuator and feedback control gain for vibration suppression of simply supported beam by minimizing the equivalent total mechanical energy of the system. However, they did not consider input energy in the used objective function i.e. equivalent total mechanical energy as such did not show the actuators voltages. This type of chromosome representation used will not be feasible for multi-input system with more sensors and actuators and it will also lead more trial and error to impose bound for the entire feedback control gain matrix elements. Wang and Quek [22] addressed the topology optimization of collocated sensors/actuators pairs for torsional vibration control of a laminated composite cantilever plate using output feedback control. They used binary-coded GA for optimization, which is not computationally efficient for actuator/sensor location in terms of number of function evaluations, and generations for convergence. Liu et al. [23] used a spatial H_2 norm of the closed-loop transfer matrix for finding the optimal nodal points for sensing displacement and applying actuation for the control of a fixed–fixed plate. This method does not address a complete coupled electromechanical analysis and uses binary-coded GA leading to very large number of generations for convergence. Authors also did not show the control input for displacement attenuation using four actuators. Swann and Chattopadhyay [24] developed an optimization procedure to detect arbitrarily located discrete delamination in composite plates using distributed piezoelectric sensors. They used GA to place sensors at the correct locations, so that the voltage signals received from the sensor set can be used to detect both the presence and the extent of damage.

GAs have also been advantageously used for optimal sensors deployment in communication network by few researchers. Buczak et al. [25] investigated the performance of GA for optimization of the sensor network by maximizing the tracking precision and minimizing the power consumption. Habib [26] modeled the coverage problem in wireless sensor network as two sub-problems such as floor plan and placement by reducing design space into discrete design space by assigning sensors into the divided cells. Author applied GA to search design space and used object-oriented class with explicit data representation rather than classical string of binary values to eliminate both encoding and decoding. Wu et al. [27] adopted a probabilistic sensing model to characterize sensors real performance in terms of coverage range, detection quality, and deployment cost and used GA to solve this optimization problem and adopted a two-dimensional numeric encoding to make up the chromosomes. Hussain et al. [28] investigated intelligent techniques for cluster formation and management and they used binary-coded GA to create energy efficient cluster for data dissemination in wireless sensor networks.

Even though many works have been reported in the broad area of active vibration control of smart structures, there are still scopes and need for improvement in better actuation and superior control

performance. Most of existing literature have used LQR control scheme for optimal control of smart structures where [Q] and [R] matrices have selected by trial and error method. Existing literatures in optimal placement of sensors/actuators have used binary-coded GA, which requires large number of generations and function evaluations for reaching near optimal solution. Most of the published work in optimal placement of piezo-patches also did not mention about the required input voltage of the actuators. However for PZTs it is very important to assure that the input voltage of the actuators are kept within the limit while maximizing the control performance. A need has therefore been felt to develop an improved GA-based combined optimal actuator placement and optimal controller design for active vibration control of such structures so that the control performance could be maximized in terms of increased closed-loop damping ratio while ensuring that the input voltages required for the actuation are within the limit of breakdown voltage of PZTs used. In the present work, thus, an improved integer-coded GA-based optimal placement of actuators have been developed in conjunction with a layered shell finite element (for analysis of thick and thin curved smart shell structures) supported by a real-coded GA-based improved LQR control scheme for superior control performance of the smart shell structures. The combined GA-based optimal placement and optimal control modules show superior performance compared to conventional optimal controllers, and the efficacy of optimal placement of actuators could be better substantiated by the use of GA-based LQR control scheme.

2. Problem definition

Fig. 1 shows a representation of a smart laminated structure having two thin patches of piezoelectric material bonded on the top and bottom surfaces of the base structure. One patch acts as sensor and the other as actuator. Signal from the sensor is used as a feedback reference in a closed-loop feedback control system. The control laws determine the feedback signal to be given to the actuator. In Fig. 1, $F(t)$, is the excited force, ϕ_s is the voltage generated by the sensor and ϕ_a is the voltage input to the actuator in order to control the displacement by developing effective control force.

3. Finite element formulation

In the present formulation, the kinematics has been described using a first-order shear deformation theory based on the Reissner–Mindlin assumptions. The basic assumptions made in the formulation are:

(a) straight line normal to the mid-surface may not remain straight during deformation,
(b) the strain energy corresponding to the stress component orthogonal to the mid-surface is disregarded.

Fig. 2 shows the general smart shell element with composite and piezoelectric layers. It has been assumed that the piezoelectric patches are perfectly bonded to the surface of the structure and the bonding layers are thin.

The geometry and various coordinate systems of the degenerate shell element [29] are shown in Fig. 3. The displacement components of the midpoint of the normal, the nodal coordinates, global stiffness matrices, applied force vectors are referred to the global coordinate system (X– Y– Z). A nodal coordinate system has

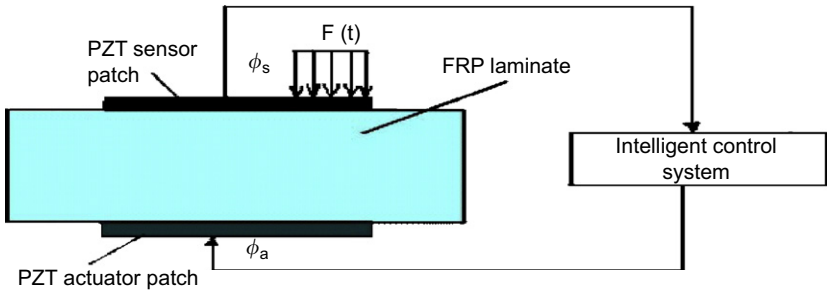

Fig. 1. Front view of a smart PZT patches bonded laminated plate with feedback control.

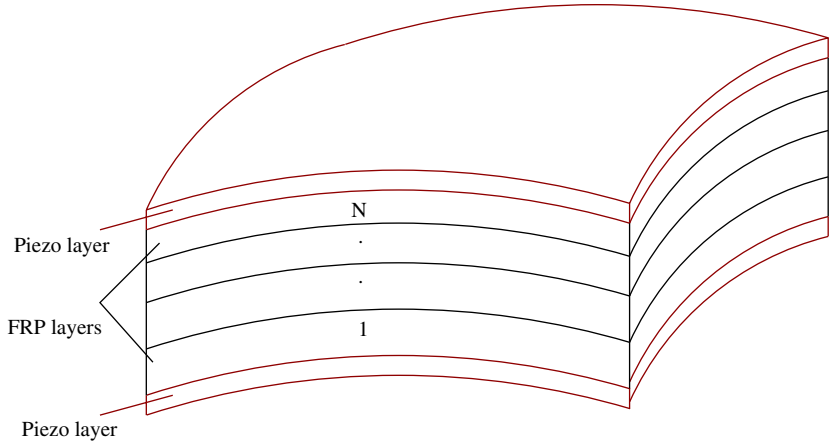

Fig. 2. Smart layered shell element.

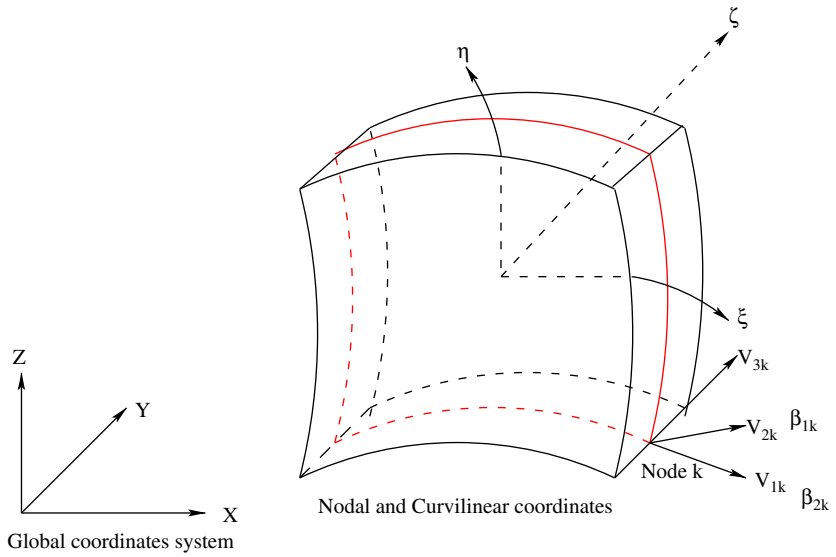

Fig. 3. Shell element with various coordinates system.

been defined by a local frame of three mutually perpendicular vectors v_1, v_2 and v_3 at each nodal point. Vector v_3 is constructed from the coordinates of the top and bottom surface at the kth node. Vector v_{1k} is perpendicular to v_{3k} and parallel to the global x–z plane or is assumed parallel to the x-axis when v_{3k} is in the y-direction. v_{2k} is derived as the cross products of v_{3k} and v_{1k}. The unit vectors in the directions of v_{1k}, v_{2k}, v_{3k} are represented by V_{1k}, V_{2k} and V_{3k}, respectively. ξ–η–ζ is a natural coordinate system, where ξ and η are the curvilinear coordinates at the middle surface, ζ is a linear coordinate in thickness direction with $\zeta = -1$ and $+1$ at the bottom and top surfaces, respectively.

3.1. Element geometry and displacement field

In the isoparametric formulation, the coordinates of a point within an element are obtained as

$$\begin{Bmatrix} x \\ y \\ z \end{Bmatrix} = \sum_{k=1}^{8} N_k(\xi,\eta) \begin{Bmatrix} x_k \\ y_k \\ z_k \end{Bmatrix}_{\text{mid}} + \sum_{k=1}^{8} N_k(\xi,\eta) \frac{h_k}{2} \zeta V_{3k} \tag{1}$$

where

$$\begin{Bmatrix} x_k \\ y_k \\ z_k \end{Bmatrix}_{\text{mid}} = \frac{1}{2}\left(\begin{Bmatrix} x_k \\ y_k \\ z_k \end{Bmatrix}_{\text{top}} + \begin{Bmatrix} x_k \\ y_k \\ z_k \end{Bmatrix}_{\text{bottom}} \right)$$

and h_k is the shell thickness at the node k.

Taking into consideration the two shell assumptions of the degeneration process, the displacement field is described by the five degrees of freedom of a normal viz. the three displacements of its mid-point $(u_k \quad v_k \quad w_k)^{\text{T}}_{\text{mid}}$ and two rotations (β_{1k}, β_{2k}). The displacements of a point on the normal resulting from the two rotations are calculated as

$$\begin{Bmatrix} u \\ v \\ w \end{Bmatrix} = \sum_{k=1}^{8} N_k \begin{Bmatrix} u_k \\ v_k \\ w_k \end{Bmatrix}_{\text{mid}} + \sum_{k=1}^{8} N_k \zeta \frac{h_k}{2} \begin{bmatrix} V_{1k}^x & -V_{2k}^x \\ V_{1k}^y & -V_{2k}^y \\ V_{1k}^z & -V_{2k}^z \end{bmatrix} \begin{Bmatrix} \beta_{1k} \\ \beta_{2k} \end{Bmatrix} \tag{2}$$

where u_k, v_k, w_k are the displacements of node k on the mid-surface along the global X, Y, Z directions, respectively, and N_K is the shape function at kth node.

3.2. Strain–displacement relations

Neglecting normal strain component in the thickness direction, the five strain components in the local coordinate system are given by

$$[\varepsilon] = \begin{bmatrix} \varepsilon_{x'} \\ \varepsilon_{y'} \\ \gamma_{x'y'} \\ \gamma_{x'z'} \\ \gamma_{y'z'} \end{bmatrix} = \begin{bmatrix} \dfrac{\partial u'}{\partial x'} \\ \dfrac{\partial v'}{\partial y'} \\ \dfrac{\partial u'}{\partial y'} + \dfrac{\partial v'}{\partial x'} \\ \dfrac{\partial u'}{\partial z'} + \dfrac{\partial w'}{\partial x'} \\ \dfrac{\partial v'}{\partial z'} + \dfrac{\partial w'}{\partial y'} \end{bmatrix} \tag{3}$$

The local derivatives are obtained from the global derivatives of the displacements u, v and w using the transformation matrix. The derivatives of displacements of any point in the shell space with respect to curvilinear coordinates can be determined by using the displacement field described in Eq. (2). With the displacement derivatives, the strain–displacement matrix in global coordinates can be formed. The strain–displacement equation relating the strain components $\{\varepsilon\}$ in global coordinate system to the nodal variables $\{d^e\}$ is expressed as

$$\{\varepsilon\} = \sum_{k=1}^{8} [(B_u)_k^e]\{d_k^e\} = [B_u^e]\{d^e\} \tag{4}$$

3.3. Direct and converse piezoelectric relations

The linear piezoelectric constitutive equations coupling the elastic and electric fields can be, respectively, expressed as the direct and converse piezoelectric equations given by

$$\{D\} = [e]\{\varepsilon\} + [\in][E] \tag{5}$$

$$\{\sigma\} = [C]\{\varepsilon\} - [e]^{\text{T}}\{E\} \tag{6}$$

where $\{D\}$ denotes the electric displacement vector, $\{\sigma\}$ denotes the stress vector, $\{\varepsilon\}$ denotes the strain vector and $\{E\}$ denotes the electric field vector. Further $[e] = [d][C]$, where $[e]$ comprises the piezoelectric coupling constants, $[d]$ denotes the piezoelectric constant matrix and $[\in]$ denotes the dielectric constant matrix.

3.4. Electrical potential in the piezoelectric patch

The element has been assumed with one electrical degree of freedom at the top of the piezoelectric actuator and sensor patches, ϕ_a^e and ϕ_s^e, respectively. Electrical potential has been assumed to be constant over an element and vary linearly through the thickness of piezoelectric patch. For a thin piezoelectric patch, the component of the electric field in the thickness direction is dominant. Therefore, the electric field can be accurately approximated with a non-zero component only in the thickness direction. With this approximation, the electric field strengths of an element in terms of the electrical potential for the actuator and the sensor patches, respectively, are expressed as

$$\{-E_a^e\} = [B_a^e]\{\phi_a^e\} = \begin{bmatrix} 0 \\ 0 \\ \frac{1}{h_a} \end{bmatrix} \{\phi_a^e\} \tag{7}$$

$$\{-E_s^e\} = [B_s^e]\{\phi_s^e\} = \begin{bmatrix} 0 \\ 0 \\ \frac{1}{h_a} \end{bmatrix} \{\phi_s^e\} \tag{8}$$

where subscripts a and s refer to the actuator patch and the sensor patch, respectively. The superscript e denotes the parameter at the element level. $[B_a^e]$ and $[B_s^e]$ are the electric field gradient matrices of the actuator and the sensor elements, respectively. It should be noted that the electric potential is introduced as an additional degree of freedom on an element level.

3.5. Dynamic finite element equations

After the application of the variational principle and finite element discretization, the coupled finite element matrix equation derived for a one-element model becomes

$$\begin{pmatrix} [M_{uu}^e] & [0] & [0] \\ [0] & [0] & [0] \\ [0] & [0] & [0] \end{pmatrix} \begin{Bmatrix} \{\ddot{d}\} \\ \{\ddot{\phi}_a\} \\ \{\ddot{\phi}_s\} \end{Bmatrix} + \begin{pmatrix} [K_{uu}^e] & [K_{ua}^e] & [K_{us}^e] \\ [K_{au}^e] & [K_{aa}^e] & [0] \\ [K_{su}^e] & [0] & [K_{ss}^e] \end{pmatrix} \begin{Bmatrix} \{d\} \\ \{\phi_a\} \\ \{\phi_s\} \end{Bmatrix} = \begin{Bmatrix} \{F^e\} \\ \{G^e\} \\ \{0\} \end{Bmatrix} \tag{9}$$

Considering a laminate made up of N layers with a total thickness of T (as shown in Fig. 2), the elemental mass and transformed stiffness matrices can be written as

Structural mass:

$$[M_{uu}^e] = \int_V \rho [N^{\mathrm{T}}][N] \, \mathrm{d}V$$

Structural stiffness:

$$[K_{uu}^e] = \frac{2}{T} \int_{-1}^{1} \int_{-1}^{1} \sum_{k=1}^{N} \frac{t_k - t_{k-1}}{2} \int_{-1}^{1} [B_u]^{\mathrm{T}} [C][B_u] |J| \, \mathrm{d}\xi \, \mathrm{d}\eta \, \mathrm{d}\zeta \tag{10}$$

Dielectric conductivity:

$$[K_{ss}^e] = -\frac{2}{T} \int_{-1}^{1} \int_{-1}^{1} \sum_{k=1}^{N} \frac{t_k - t_{k-1}}{2} \int_{-1}^{1} [B_\phi]^{\mathrm{T}} [\in][B_\phi] |J| \, \mathrm{d}\xi \, \mathrm{d}\eta \, \mathrm{d}\zeta \tag{11}$$

Piezoelectric coupling matrix:

$$[K_{us}^e] = \frac{2}{T}\int_{-1}^{1}\int_{-1}^{1}\sum_{k=1}^{N}\frac{t_k - t_{k-1}}{2}\int_{-1}^{1}[B_u]^{\mathrm{T}}[e]^{\mathrm{T}}[B_\phi]|J|\,\mathrm{d}\xi\,\mathrm{d}\eta\,\mathrm{d}\zeta \tag{12}$$

Stiffness matrices have been evaluated by numerical integration using Gauss quadrature ($3\times3\times2$) scheme or ($2\times2\times2$) selective integration scheme depending on the shell thickness. After assembling the elemental stiffness matrices, the global set of equations become

$$[M_{uu}]\{\ddot{d}\} + [K_{uu}]\{d\} + [K_{ua}]\{\phi_a\} = \{F\} \tag{13}$$

$$[K_{au}]\{d\} + [K_{aa}]\{\phi_a\} = \{G\} \tag{14}$$

$$[K_{su}]\{d\} + [K_{ss}]\{\phi_s\} = 0 \tag{15}$$

For open electrodes, charge can be expressed as

$$\{G\} = 0 \tag{16}$$

After substituting Eqs. (14) and (15) into Eq. (13), the overall dynamic finite element equation can be expressed as

$$[M_{uu}]\{\ddot{d}\} + [[K_{uu}] - [K_{ua}][K_{aa}]^{-1}[K_{au}] - [K_{us}][K_{ss}]^{-1}[K_{su}]]\{d\} = \{F\} - [K_{ua}]\{\phi_a\} \tag{17}$$

where $[M_{uu}]$ is the global mass matrix, $[K_{uu}]$ is the global elastic stiffness matrix, $[K_{ua}]$ and $[K_{us}]$ are the global piezoelectric coupling matrices of actuator and sensor patches, respectively. $[K_{aa}]$ and $[K_{ss}]$ are the global dielectric stiffness matrices of actuator and sensor patches, respectively.

3.6. State-space representation

Lower order modes of vibration have lower energy associated and consequently are the most easily excitable ones. These are the most significant to the global response of the system. A truncated modal matrix ψ can be utilized as a transformation matrix between the generalized coordinates $d(t)$ and the modal coordinates $\eta(t)$. Thus the displacement vector $d(t)$ can be approximated by the modal superposition of the first 'r' modes as

$$\{d(t)\} \approx [\psi]\{\eta(t)\} \tag{18}$$

where $[\psi] = [\psi_1\ \psi_2\ \ldots\ \psi_r]$ is the truncated modal matrix.

The decoupled dynamic equations considering modal damping can be written as

$$\left\{\ddot{\eta_i}(t)\right\} + 2\xi_{di}\omega_i\left\{\dot{\eta_i}(t)\right\} + \omega_i^2\{\eta_i(t)\} = [\psi]^{\mathrm{T}}\{F\} - [\psi]^{\mathrm{T}}[K_{ua}]\{\phi_a\} \tag{19}$$

where ξ_{di} is the damping ratio.

Eq. (19) can be represented in state-space form as

$$\{\dot{X}\} = [A]\{X\} + [B]\{\phi_a\} + [\hat{B}]\{u_d\} \tag{20}$$

$$[A] = \begin{bmatrix} [0] & [I] \\ [-\omega_i^2] & [-2\xi_{di}\omega_i] \end{bmatrix}$$

is the system matrix,

$$[B] = \begin{bmatrix} [0] \\ -[\psi]^{\mathrm{T}}[K_{ua}] \end{bmatrix}$$

is the control matrix,

$$[\hat{B}] = \begin{bmatrix} [0] \\ [\psi]^{\mathrm{T}}\{F\} \end{bmatrix}$$

is the disturbance matrix, $\{u_d\}$ is the disturbance input vector, $\{\phi_a\}$ is the control input, and

$$\{\dot{X}\} = \begin{Bmatrix} \dot{\eta} \\ \ddot{\eta} \end{Bmatrix} \quad \text{and} \quad \{X\} = \begin{Bmatrix} \eta \\ \dot{\eta} \end{Bmatrix} \tag{21}$$

The sensor output equation can be written as

$$\{y\} = [C_0]\{X\} \tag{22}$$

where output matrix $[C_0]$ depends on the modal matrix $[\psi]$ and the sensor coupling matrix $[K_{us}]$.

4. Controllability index for actuator location

The system controllability is a basis in the modern control theory. Wang and Wang [7] proposed a controllability index for actuator locations, which was obtained by maximizing the global control force, and this has been considered in the present study. The modal control force f_c applied to the system can be written as

$$\{f_c\} = [B]\{\phi_a\} \tag{23}$$

It follows from Eq. (23) that

$$\{f_c\}^{\mathrm{T}}\{f_c\} = \{\phi_a\}^{\mathrm{T}}[B]^{\mathrm{T}}[B]\{\phi_a\} \tag{24}$$

Using the singular value analysis, $[B]$ can be written as $[B] = [M][S][N]^{\mathrm{T}}$, where $[M]^{\mathrm{T}}[M] = [I]$, $[N]^{\mathrm{T}}[N] = [I]$ and

$$[S] = \begin{bmatrix} \sigma_1 & \dots & 0 \\ 0 & \ddots & \vdots \\ \vdots & \dots & \sigma_{n_a} \\ 0 & \dots & 0 \end{bmatrix}$$

where n_a is the number of actuator. Eq. (24) can be rewritten as

$$\{f_c\}^{\mathrm{T}}\{f_c\} = \{\phi_a\}^{\mathrm{T}}[N][S]^{\mathrm{T}}[S][N]^{\mathrm{T}}\{\phi_a\}$$

or

$$\left\|\{f_c\}\right\|^2 = \left\|\{\phi_a\}\right\|^2 \|S\|^2 \tag{25}$$

Thus, maximizing this norm independently on the input voltage $\{\phi_a\}$ induces maximizing $\|S\|^2$. The magnitude of σ_i is a function of location and the size of piezoelectric actuators. Wang and Wang [7] proposed that the controllability index is defined by

$$\Omega = \prod_{i=1}^{n_a} \sigma_i \tag{26}$$

The higher the controllability index, the smaller will be the electrical potential required for control.

5. LQR optimal feedback

LQR optimal control theory has been used to determine the control gains. In this, the feedback control system has been designed to minimize a cost function or a performance index, which is proportional to the required measure of the system's response. The cost function used in the present case is

given by

$$J = \frac{1}{2}\int_{t_0}^{t_f} (\{y\}^{\mathrm{T}}[Q]\{y\} + \{\phi_a\}^{\mathrm{T}}[R]\{\phi_a\})\,\mathrm{d}t \tag{27}$$

where $[Q]$ and $[R]$ are the semi-positive-definite and positive-definite weighting matrices on the outputs and control inputs, respectively.

The steady-state matrix Ricatti equation can be written as

$$[A]^{\mathrm{T}}[K] + [K][A] - [K][B][R]^{-1}[B]^{\mathrm{T}}[K] + [C]^{\mathrm{T}}[Q][C] = 0 \tag{28}$$

After solving the Ricaati equation using Potters method, optimal gain can be written as

$$[G_c] = [R]^{-1}[B]^{\mathrm{T}}[K] \tag{29}$$

Considering output feedback, actuation voltage can be calculated as

$$\{\phi_a\} = -[G_c]\{y\} \tag{30}$$

5.1. Determination of weighting matrices

Weighting matrices $[Q]$ and $[R]$ are important components of LQR optimization process. The compositions of $[Q]$ and $[R]$ elements influence the system's performance. Lewis [30] assumed $[Q]$ and $[R]$ to be a semi-positive-definite and positive-definite matrices, respectively. Ang et al. [11] proposed that $[Q]$ and $[R]$ matrices could be determined considering weighted energy of the system as follows:

$$[Q] = \begin{bmatrix} \alpha_2[\psi]^{\mathrm{T}}[K][\psi] & [0] \\ [0] & \alpha_1[\psi]^{\mathrm{T}}[M][\psi] \end{bmatrix} \text{ and } [R] = \gamma[\hat{R}] \tag{31}$$

The proposed weighted energy of the system in the quadratic form is

$$\prod\!\!\!\!\!\prod = \tfrac{1}{2}\alpha_1\{\dot{X}\}^{\mathrm{T}}[M]\{\dot{X}\} + \tfrac{1}{2}\alpha_2\{X\}^{\mathrm{T}}[K]\{X\} + \tfrac{1}{2}\gamma\{\phi_a\}^{\mathrm{T}}[\hat{R}]\{\phi_a\} \tag{32}$$

where $[\hat{R}]$ is the dielectric coupling matrix of the actuators and α_1, α_2 and γ are the coefficients associated with total kinetic energy, strain energy and input energy, respectively. These coefficients will take different values in the control algorithm apart from the value of unity to allow for the relative importance of these energy terms. The closed-loop damping values can be calculated by using the following equation:

$$\ln\left(\frac{x_i}{x_{i+1}}\right) = \frac{2\pi\xi_d}{\sqrt{(1-\xi_d^2)}} \tag{33}$$

Therefore, a search algorithm is required for finding $[Q]$ and $[R]$ by taking α_1, α_2 and γ as variables, which will give maximum control response within the allowable actuators voltage. In this present study, optimization problem has been proposed as follows:

$$\xi_{d\,\max} = \frac{1}{\sqrt{(1+(4\pi^2/p^2))}} \tag{34}$$

subjected to

$$\phi_i < \phi_{\max}, \quad i = 1, \ldots, n_a \tag{35}$$

where $p = \ln(x_i/x_{i+1})$, n_a is the number of actuators and $\phi_{\max}$ refers to the maximum voltage that can be applied on the actuators depending on the piezoelectric materials and thickness of the piezolayers. The allowable voltage of piezo-ceramic materials is around 500–1000 V per 1 mm piezo-thickness [31].

6. Genetic algorithms

GA is a powerful and broadly applicable stochastic search and optimization technique based on the principles of natural selection and genetics. GA begins with a population of randomly generated candidates and evolves towards a solution by applying genetic operators such as reproduction, crossover and mutation. These algorithms are highly parallel, guided, random adaptive search techniques. In the present study, two types of GAs have been used for optimal placement of actuators and finding $[Q]$ and $[R]$ matrices. In the following subsections, these algorithms have been briefly described.

6.1. Integer-coded GA

GA is an influential tool for the solution of combinatorial problems such as the actuator placement problem. For this problem the design variables are the positions of the actuators. The most natural representation is a string of integers specifying the locations of actuators.

The gene code is taken as ac_1, ac_2, …, ac_j, …, ac_{na}, where $ac_j \in (1, m)$ and is a positive integer number, where m is the total locations for actuators in the structures/system. Uniform crossover and a new mutation technique for integer-coded GA have been discussed in the following subsections.

6.1.1. Uniform crossover

The steps involve in this crossover are

(a) a random mask is generated,
(b) the mask determines which bits are copied from one parent and which from the other parent,
(c) bit density in mask determines how much material is taken from the other parent.

For example, if the randomly generated mask is 0110011000 and parents are 1010001110 and 0011010010 then their offspring will be 0011001010 and 1010010110.

6.1.2. Mutation

A one-digit positive integer value $ac_j \in [1, m]$ is generated randomly, which replaces the old one when mutating. If ac_j is equal to old one then a new positive integer is selected again until they are different in the chromosome. The efficiency of the mutation could be improved greatly using the method.

6.2. Real-coded GA

In the present study, real-coded GA along with SBX and parameter-based mutation [18] operators have been used for finding $[Q]$ and $[R]$ matrices in LQR control scheme. In the following subsections, these operators have been briefly described.

6.2.1. Simulated binary crossover

A probability distribution function has been used around the parent solutions to create two children solutions as

$$P(\beta) = \begin{cases} 0.5(\eta_c + 1)\beta^{\eta_c} & \text{if } \beta \leqslant 1 \\ 0.5(\eta_c + 1)/\beta^{\eta_c + 2} & \text{otherwise} \end{cases} \tag{36}$$

where

$$\beta = \left| \frac{b^{(2)} - b^{(1)}}{a^{(2)} - a^{(1)}} \right|$$

and $b^{(1)}$, $b^{(2)}$ are the children solutions, and $a^{(1)}$, $a^{(2)}$ are the parent solutions. η_c is a parameter which controls the extent of spread in children solution. A small value of η_c allows solutions far away from parents to be

created as children solutions and a large value restricts only near-parent solutions to be created as children solutions. In the most of the literature, the small and large values of η_c are taken as 2 and 5, respectively [18]. A self-adaptive procedure for updating η_c parameter can also be used for calculating this parameter [32]. The procedure adopted for computing children solution $b^{(1)}$and $b^{(2)}$ from parent solutions $a^{(1)}$ and $a^{(2)}$ are as follows:

1. A random number u between 0 and 1 has been generated.
2. Parameter $\bar{\beta}$ has been found using the polynomial probability distribution (Eq. (36)) and $\bar{\beta}$ can be written as

$$\bar{\beta} = \begin{cases} (\alpha u)^{1/\eta_c+1} & \text{if } u \leqslant 1/\alpha \\ (\frac{1}{2} - \alpha u)^{1/\eta_c+1} & \text{otherwise} \end{cases} \tag{37}$$

where $\alpha = 2 - \beta^{-(\eta_c+1)}$ and β is calculated as follows:

$$\beta = 1 + \frac{2}{a^{(u)} - a^{(l)}} \min[(a^{(1)} - a^{(l)}), (a^{(u)} - a^{(2)})] \tag{38}$$

where a^l and a^u are lower and upper bounds of a variable.

The children solutions are then calculated as follows:

$$b^{(1)} = 0.5[(a^{(1)} + a^{(2)}) - \bar{\beta}|a^{(2)} - a^{(1)}|] \tag{39}$$

$$b^{(2)} = 0.5[(a^{(1)} + a^{(2)}) + \bar{\beta}|a^{(2)} - a^{(1)}|] \tag{40}$$

6.2.2. Parameter-based mutation operator

A polynomial probability distribution has been used to create a solution b in the vicinity of a parent solution and following procedure has been used:

1. A random number u between 0 and 1 has been generated.
2. The parameter $\bar{\delta}$ is calculated as follows:

$$\bar{\delta} = \begin{cases} [2u + (1-2u)(1-\delta)^{\eta_m+1}]^{1/\eta_m+1} - 1 & \text{if } u \leqslant 0.5 \\ \left(1 - [2(1-u) + 2(u-0.5)(1-\delta)^{\eta_m+1}]^{1/\eta_m+1}\right) & \text{otherwise} \end{cases} \tag{41}$$

where $\delta = \min[(a-a^l), (a^u-a)]/(a^u-a^l)$, η_m is the distribution index for the mutation and takes any non-negative value.
3. The mutated child is calculated as follows:

$$b = a + \bar{\delta}\Delta_{\max} \tag{42}$$

where $\Delta_{\max}$ is maximum perturbation allowed in the parent solution. By setting $\Delta_{\max} = a^u - a^l$, the expected normalized perturbation can be calculated from Eq. (42) as

$$(b - a)/(a^u - a^l)$$

It has been observed that this value is $O(1/\eta_m)$ [18]. Thus, in order to get a mutation effect of 1% perturbation η_m has been taken as 100.

6.3. Optimal actuator location using GA

The distribution of actuators influences the control of structural vibration and this leads to the problem of optimal selection of actuator locations for achieving best control. GA could be advantageously used for optimal actuators placement problem, where the design variables are the positions of the actuators. However,

use of binary-coded GA increases the size of the string/chromosome. Furthermore, most mutations and crossovers result in designs with the wrong number of actuators and it will also increase the number of function evaluations. So, the most natural representation is a string of integers specifying the locations of actuators. Hence, in this study, integer-coded GA with uniform crossover and mutation have been developed for optimal placement of actuators. The outline of optimization problem using GA is as follows:

(i) Initial chromosomes depending on the number of actuators and populations are chosen randomly.
(ii) Fitness value (measure of controllability) is calculated for each chromosome.
(iii) Genetic operators are applied to produce a new set of chromosomes.
(iv) Steps (ii)–(iii) are repeated until the fitness converges.
(v) Computation is terminated after the convergence of fitness and the chromosome based on the best controllability value is selected as the optimal locations of actuators.

6.4. The GA approach to optimal LQR

The design of optimal LQR involves finding out the control gain, G_c such that performance index J (Eq. (27)) for the system represented by Eq. (19) is minimized. Weighting matrices in Eq. (27) have to be decided by the designer's choice. The optimal gain, G_c in Eq. (29) can be obtained by solving Riccati equation (28). However, it is not a trivial problem to find the optimal gain since the control performance depends on the choice of weighting matrices. In the present work, weighting matrices have been determined by the genetic search to obtain best control gain for the optimal LQR scheme. Parameters α_1, α_2 and γ in Eq. (31) have been represented by real-valued genes for finding $[Q]$ and $[R]$ matrices. The population size in the present problem has been taken as 10. The fitness value has been calculated with respect to each chromosome using the following expression:

$$\xi_d = \begin{cases} \left(\dfrac{1}{\sqrt{1+(4\pi^2/p^2)}}\right) & \text{if } \phi_i < \phi_{\max} \\ \left[10^{-8} \times \left(\dfrac{1}{\sqrt{(1+(4\pi^2/p^2))}}\right)\right] & \text{otherwise} \end{cases} \tag{43}$$

The ranges of α_1, α_2 and γ are taken as $0<\alpha_1\leqslant 200$, $0<\alpha_2\leqslant 200$ and $0<\gamma\leqslant 2$ where controlled response depends on α_1, α_2 and γ. Parents have been selected through roulette wheel operator and offspring have been created using SBX and polynomial mutation operator [18]. The distribution parameters associated with SBX and polynomial mutation operator have been taken as $\eta_c = 2$ and $\eta_m = 100$. Genetic evolution has been continued for large number of generations till the fitness converges. Fig. 4 shows the steps in determining the weighting matrices for optimal gain by real-coded GA in the present problem.

7. Results and discussion

Based on the formulations discussed in the previous sections, a complete computer code has been developed for finite element analysis of smart shell structures followed by optimal actuator placement and LQR control using GA.

7.1. Structural validation

In order to verify the finite element code developed, a spherical shell made of graphite/epoxy with the four edges simply supported, having the following dimensions have been considered: $a/b = 1$, $R_1 = R_2 = R$, $R/a = 3$, $a/h = 10$. Graphite/epoxy properties considered are as follows: $E_1 = 25E_2$, $G_{12} = G_{13} = 0.5E_2$, $\upsilon_{12} = 0.25$, $G_{23} = 0.2E_2$. A 10×10 finite element mesh has been used to model this entire shell. Non-dimensionalized central deflection (w^a) of laminated spherical shell under point load $P = 10\,\mathrm{N}$ at the center and non-dimensionalized fundamental frequency (λ^{**}) have been calculated from the present code are listed in

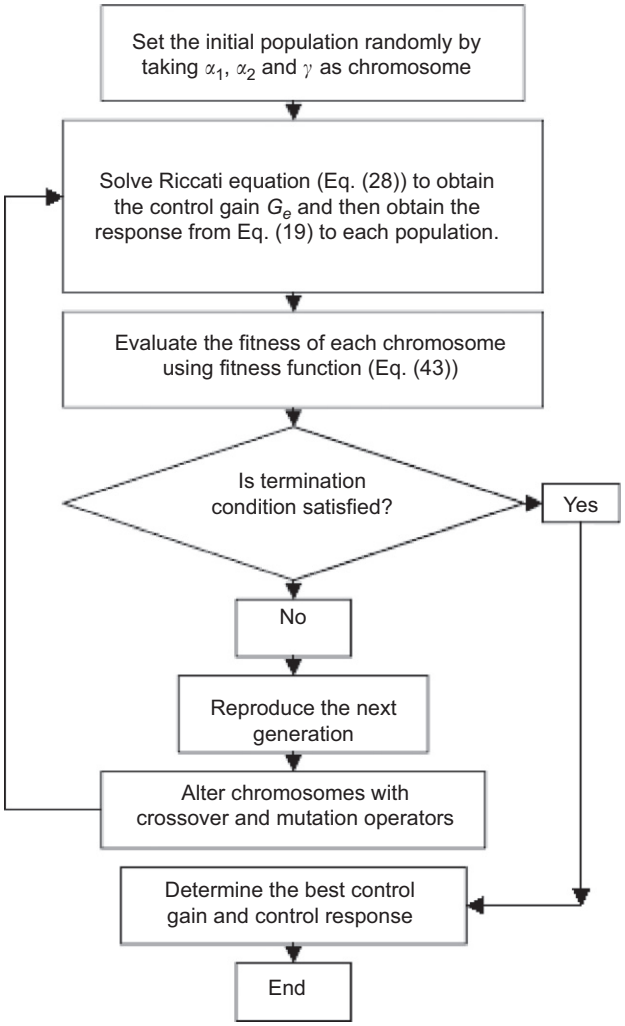

Fig. 4. Flowchart of GA-based LQR.

Table 1 along with exact solution of Reddy [33] as

$$w^a = (wh^3E_2/Pa^2) \times 10^2$$

$$\lambda^{**} = \frac{\lambda a^2}{h}\sqrt{\rho/E_2}$$

It could be observed that the results obtained from the present finite element code are in close agreement with the exact solution [33].

7.2. Electro-mechanical validation

In order to verify the accuracy of the present coupled electro-mechanical finite element code, the results obtained from the present code have been compared with the benchmark problem proposed by Hwang and Park [34]. Here, a cantilever bimorph (as shown in Fig. 5) made of two PVDF layers laminated together has been considered subjected to an external voltage. The induced internal stresses result in a bending moment which forces the bimorph beam to bend. The bimorph beam has been discretized into five elements. The dimensions of the beam are length, $L = 100$ mm, width, $W = 5$ mm and thickness, $h = 1$ mm. The analytical

Table 1
Comparison of non-dimensionalized central deflection and fundamental frequency for different laminates

Stacking sequence	Center deflection from		Fundamental frequency from	
	Present code	Reddy [33]	Present code	Reddy [33]
0/90	6.5030	6.5444	9.2560	9.9608
0/90/0	5.0709	4.9546	11.8501	12.731
[0/90]$_s$	4.5871	4.7579	11.9823	12.795

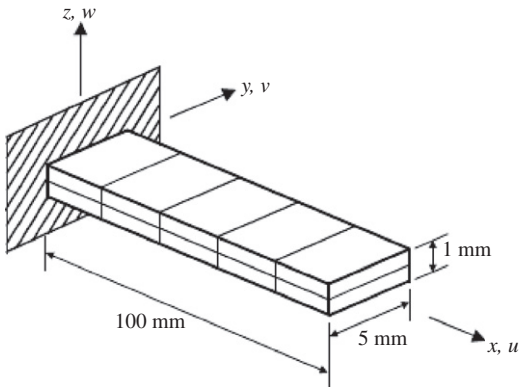

Fig. 5. Schematic view of a bimorph beam.

Table 2
Transverse deflections of piezoelectric bimorph actuator

Distance (mm) from fixed end	Deflection (μm) Tzou and Ye [35] (theory)	Deflection (μm) Chee et al [36] (FEM)	Deflection (μm) Hwang and Park [34]	Deflection (μm) present FEM
20	0.0138	0.0138	0.0131	0.0136
40	0.0552	0.0552	0.0545	0.0540
60	0.1240	0.1242	0.1200	0.1223
80	0.2210	0.2208	0.2180	0.2181
100	0.3450	0.3450	0.3400	0.3416

solution to transverse displacement w is given by [35]

$$w = 1.5\frac{e_{31}\phi}{Eh^2}x^2 \tag{44}$$

A unit voltage has been applied across the thickness and the calculated transverse deflections of five nodes have been compared with the results of Hwang and Park [34], Tzou and Ye [35] and Chee et al. [36] as shown in Table 2 and excellent agreements have been achieved.

7.3. Validation for optimal actuators placement

A smart fiber reinforced polymer (FRP) cantilever beam made of GR/E has been considered to validate the code for optimal placement of actuators as well as to compare the performances of integer and binary-coded GA in terms of generation required to reach the optimal solution. In this analysis, four actuators and first

mode of vibration have been considered. The length and width of the beam are taken as 0.2 and 0.01 m, respectively. The stacking sequence of the laminated beam structure considered is $[p/[0/0]_s/p]$. Here 'p' stands for piezo-patches one for sensing and the other for actuation. Thickness of each ply has been considered as 0.15 mm and that of piezo-patch is 0.5 mm. The mechanical, electrical and coupled material properties [9] used in the present study have been listed in Table 3. Several important parameters used for integer- and binary-coded GA have been listed in Table 4. Optimal actuators placement based on the maximum controllability index is shown in Fig. 6. It could be clearly observed from Fig. 6 that the optimal locations of PZT actuators are at the root of the beam. This result is expected since the curvature of the first mode of vibration reaches its maximum value at the fixed end of the cantilever beam and a similar observation was also reported by Wang and Wang [7]. Fig. 7 shows the convergence plot with number of generations for integer-coded and binary-coded GA and it could be observed that while the integer-coded GA converges at 31 generations, binary-coded GA converges only after 246 generations.

Table 3
Material properties of structural laminae and PZT

Material properties	Structural laminae	PZT
E_1	172.5 GPa	63.0 GPa
$E_2 = E_3$	6.9 GPa	63.0 GPa
$G_{12} = G_{13}$	3.45 GPa	24.6 GPa
G_{23}	1.38 GPa	24.6 GPa
$\upsilon_{12} = \upsilon_{13} = \upsilon_{23}$	0.25	0.28
ρ	1600 kg m^{-3}	7600 kg m^{-3}
$e_{31} = e_{32}$	0.0	10.62 C m^{-2}
$\in_{11} = \in_{22} = \in_{33}$	0.0	0.1555×10^{-7} F m^{-1}

Table 4
Several important parameters for integer- and binary-coded GA

	Integer-coded GA	Binary-coded GA
Number of genes to represent		
One actuator	1	8
Length of the chromosome	4	32
Population size	10	10
Crossover probability	0.9	0.9
Mutation probability	0.1	0.1

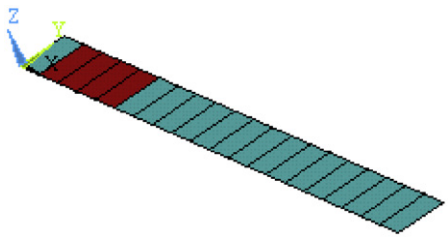

Fig. 6. Optimal location of four actuators on the beam substrate based on maximum controllability.

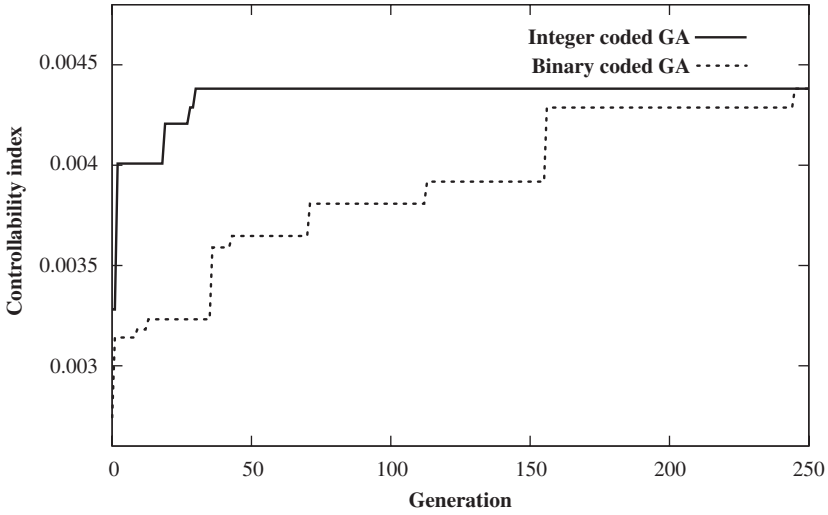

Fig. 7. Comparison of variation of controllability index with generation for the cantilever beam using integer- and binary-coded GA.

7.4. Optimal vibration control using GA-LQR scheme

After validation of the developed code, two types of smart FRP laminated structures have been considered to study the optimal placement of actuators and vibration control of such structures. In all the cases, thickness of each piezoelectric patch has been considered as 0.5 mm and the allowable voltage has been taken as 500 V [31]. In the present study, first the optimal placement of actuators using GA and subsequent control using GA-LQR control scheme has been applied for the control of

(i) a smart spherical shell panel and
(ii) a smart cylindrical shell panel

subjected to an impulse applied load. In all the cases, optimal actuators placement and dynamic responses of the piezo-laminated structures have been calculated considering the first eight modes. Dynamic responses of the piezo-laminated structures have been calculated using mode superposition technique. In this study, six numbers of actuators have been considered. The number of piezoelectric actuators has been assumed to be less than the number of modes to be controlled [7]. For all the cases, a modal damping ratio (ξ_d) of 1% has been assumed to obtain open loop response and to calculate LQR gains [9].

7.4.1. Optimal vibration control of laminated spherical shell panel

A simply supported smart FRP composite shell panel on a square base ($a = b = 0.04$ m) under the action of impulse load at the center has been considered. The radius (i.e. $R_1 = R_2 = R$) of this panel has been considered to be 0.12 m. The stacking sequence of the laminated spherical structure considered is $[p/[0/90]_s/p]$. Here 'p' stands for piezo-patches one for sensing and the other for actuation. Thickness of each ply has been considered to be 0.75 mm and that of piezo-patch has been taken as 0.5 mm. A 10×10 finite element mesh has been considered to model this entire panel. Two types of piezo-patch locations viz. Placement1 and Placement2 have been considered to study influence of optimal placement on the input voltage of actuator and the closed-loop damping ratio. Placement1 stands for optimal actuators placement based on the maximum controllability index considering six actuators as shown in Fig. 8. Placement2 stands for actuators placement based on the mode shapes considering eight actuators as shown in Fig. 9. Fig. 10 presents the evolution of the best fitness value i.e. controllability index using GA after 50 generations. The value of controllability index corresponding to Placement2 is 0.56991. In case of Placement1, the maximum value of controllability index is 0.680956 as shown in Fig. 10. The smart panel considering Placement1 has been subjected to an impulse load

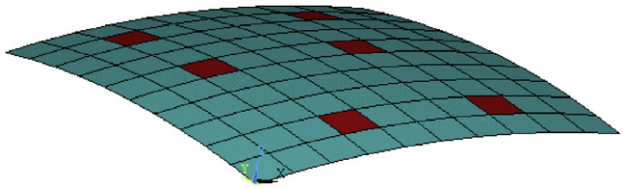

Fig. 8. Collocated sensors and actuators location on the spherical panel substrate based on maximum controllability index.

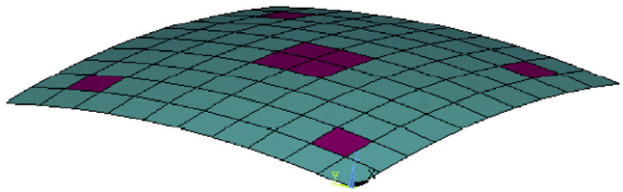

Fig. 9. Collocated sensors and actuators location on the spherical panel substrate based on the mode shapes.

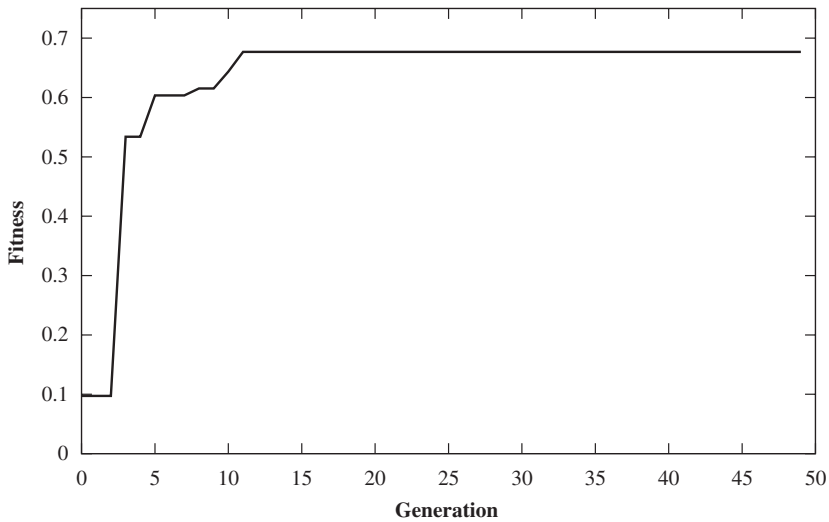

Fig. 10. Variation of controllability index with generation for spherical shell panel using Placement1.

of 10 N at the center for a duration of 4.65751 μs and impulse responses of this panel have been calculated with a time step of 1.164379 μs (time step taken as $\tau/100$ where τ is the time period corresponding to first natural frequency of the system). The smart panel considering Placement2 has also been subjected to an impulse load of 10 N at the center for duration of 4.65512 μs and impulse responses of this panel have been calculated with a time step of 1.16378 μs. Fig. 11 shows the uncontrolled displacement history of smart spherical panel. The LQR controlled displacement histories of smart spherical panel using Placement1 and Placement2 have been depicted in Fig. 12. In the simple LQR controlled response of the panel with Placement1 and Placement2, the closed-loop damping ratios achieved have been 1.18% and 1.0147% respectively. The maximum actuator voltage variations using Placement1 and Placement2 for simple LQR control scheme have been shown in Fig. 13. It could be observed from Fig. 13 that the magnitude of maximum actuator voltage is much less in the case of Placement1 compared to that in Placement2 for simple LQR control scheme even though the corresponding closed-loop damping ratios are not much different. This is due to the fact that the electromechanical coupling matrix in the case of optimal placement (Placement1) leads to better actuation.

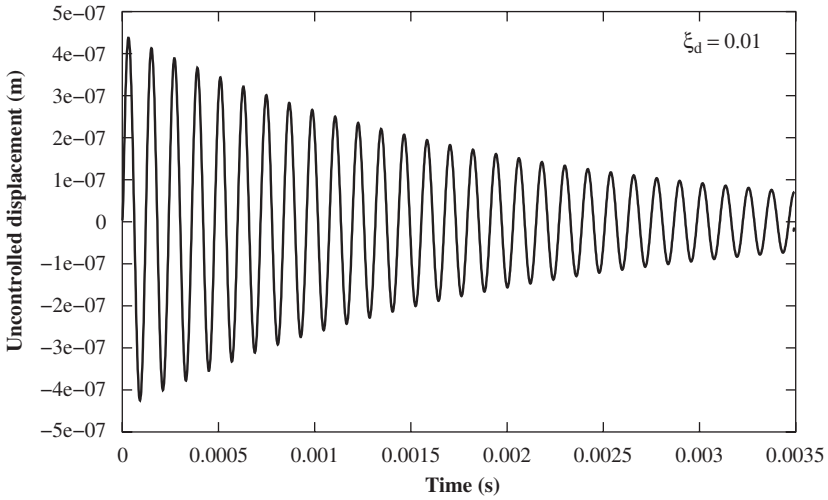

Fig. 11. Uncontrolled displacement history of the smart FRP composite spherical panel.

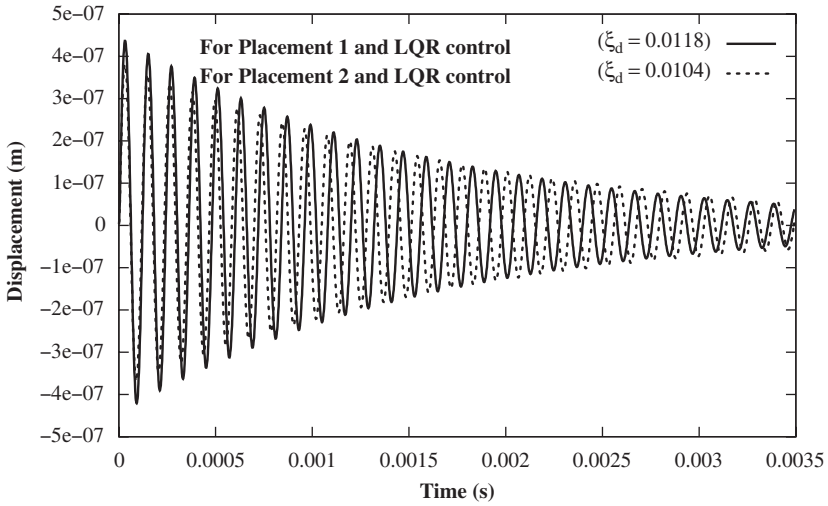

Fig. 12. LQR controlled displacement history of the smart FRP composite spherical panel.

Fig. 14 shows the GA-LQR controlled displacement histories using Placement1 and Placement2. In this case the closed-loop damping ratios achieved with Placement1 and Placement2 are 12.03% and 4.69%, respectively. It has been observed from Figs. 12 and 14 that the closed-loop damping ratio is much more in the case of GA-LQR search control scheme than that in case of simple LQR control scheme. The maximum actuator voltage variation using Placement1 and Placement2 for GA-LQR control scheme is shown in Fig. 15. It could be clearly noticed from Fig. 15 that the maximum actuator voltage is much more in the case of Placement2 compared to that in the case of Placement1 for GA-LQR search control scheme. This clearly shows that the present control scheme leads to better control performance with less input voltages of actuators. Fig. 16 shows the convergence of calculated fitness i.e. closed-loop damping ratio with number of generations using Placement1 and Placement2 for GA-LQR search control scheme. It could be observed that the closed-loop damping ratio is not only much higher in the case of Placement1 compared to that in case of Placement2, but the convergence has also been achieved much faster. From this study it could be concluded that optimal actuator placement using GA and subsequent GA-LQR control scheme lead to the maximization of closed-loop damping ratio with minimum input/actuator voltage within the limit. Optimal vibration control

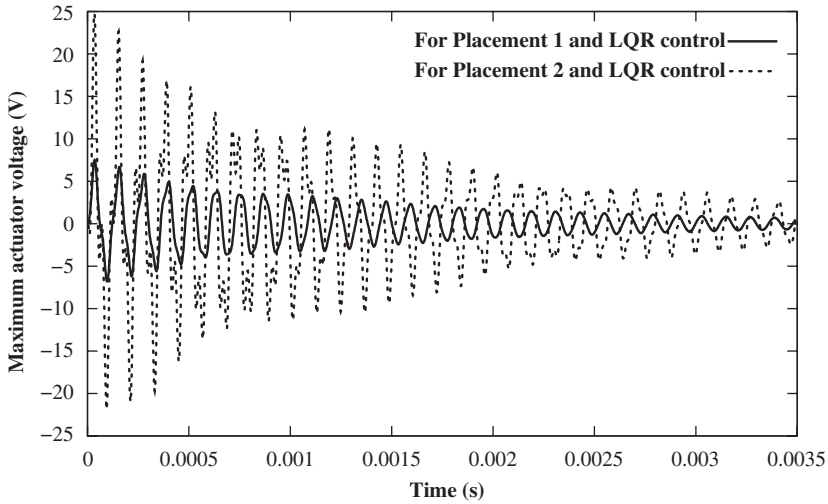

Fig. 13. Maximum actuator voltage variation for LQR control scheme of spherical panel.

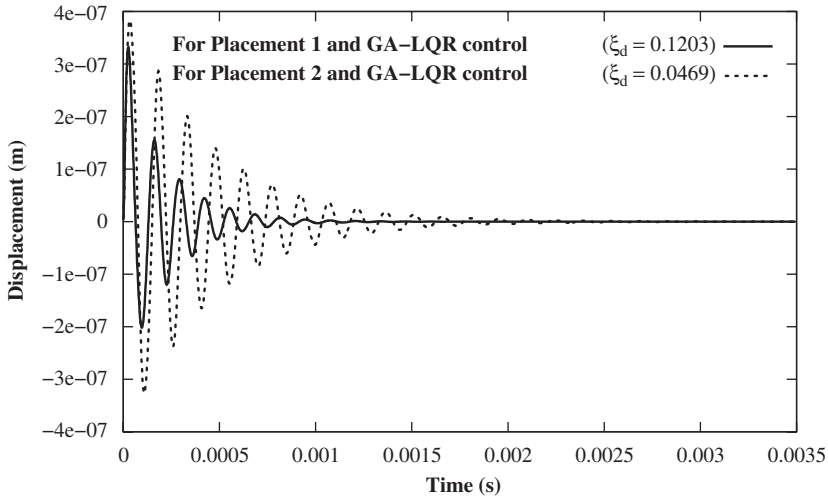

Fig. 14. GA-LQR controlled displacement history of the smart FRP composite spherical panel.

of smart cylindrical panel using optimal actuator placement based on controllability index and subsequent GA-LQR control scheme has also been discussed in the following section.

7.4.2. Optimal vibration control of laminated spherical cylindrical panel

A simply supported smart FRP composite cylindrical panel under the action of impulse load at the center has been considered. Dimensions of this panel are $a = b$, $a/h = 100$, $a/R = 0.5$, $h = 4$ mm and the stacking sequence of the laminated cylindrical shell structure has been considered as $[p/[-45/45]_s/p]$. Here 'p' stands for piezo-patches one for sensing and the other for actuation. Thickness of each ply has been considered to be 0.75 mm and that of piezo-patch has been taken as 0.5 mm. A 10×10 finite element mesh has been considered to model this entire panel. Piezo-patch locations have been determined based on the maximum controllability index. Fig. 17 presents the evolution of the best fitness value i.e. controllability index after 50 generations. The locations of actuators based on this value are shown in Fig. 18. The smart cylindrical panel has been then subjected to an impulse load of 10 N at the center for a duration of 170.496 μs. Impulse responses of the panel have been calculated with a time step of 28.416 μs (time step taken as $\tau/100$ where τ is the time period

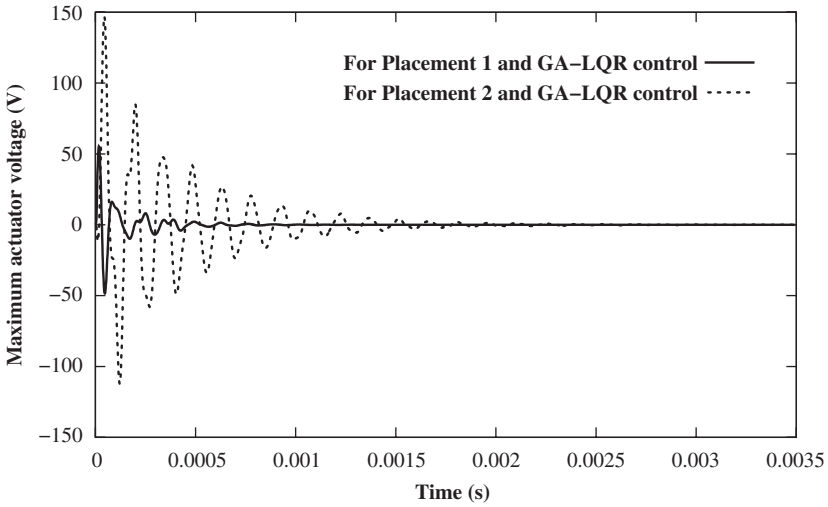

Fig. 15. Maximum actuator voltage variation for GA-LQR control scheme of spherical panel.

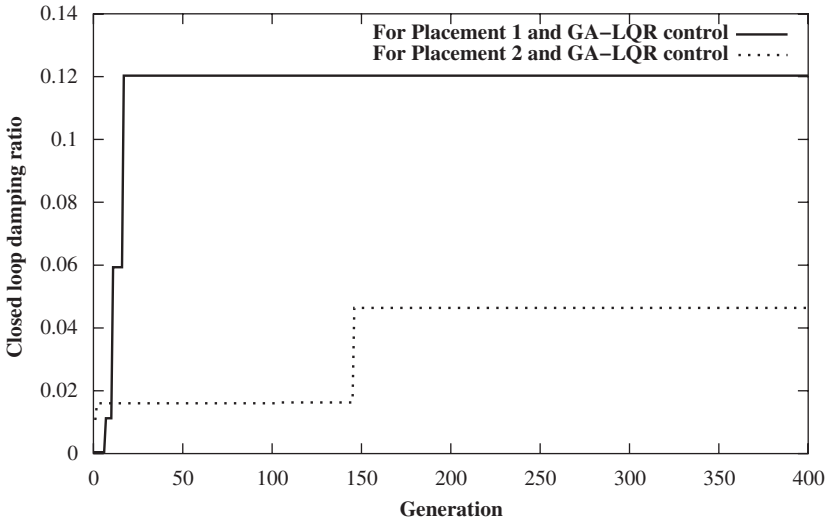

Fig. 16. Variation of closed-loop damping ratio with generation for spherical shell panel using Placement1 and Placement2 with GA-LQR control.

corresponding to first natural frequency of the system) and GA-LQR scheme has been applied to control the displacement of the panel center. Fig. 19 shows the uncontrolled, LQR controlled and GA-LQR controlled histories. It could be observed from Fig. 19 that the closed-loop damping ratio achieved with LQR controlled is 1.68% where as the closed-loop damping ratio achieved with GA-LQR controlled scheme is 8.117%. The maximum actuator voltage variations for simple LQR and GA-LQR control scheme are shown in Fig. 20 and it could be observed that input voltage required is much less in the case of GA-LQR control scheme. Fig. 21 shows the convergence of calculated fitness with number of generation.

7.4.3. Comparative performance of LQR and GA-LQR control schemes

In the present work, in all the cases considered, the dimension of $[Q]$ matrix is 16×16. For the $[R]$ matrix, the dimension is 6×6 for six actuators and 8×8 for eight actuators (while considering mode-shaped-based actuators placement). In all the cases (total six cases), relative performances have been studied in terms of effective closed-loop damping ratio and input voltage requirement for the actuators. $[Q]$ and $[R]$ matrices have

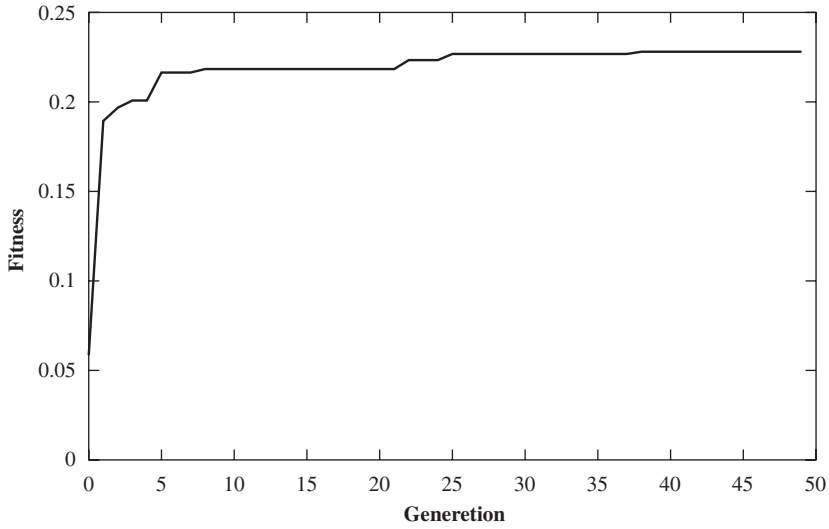

Fig. 17. Variation of controllability index with generation for cylindrical shell panel.

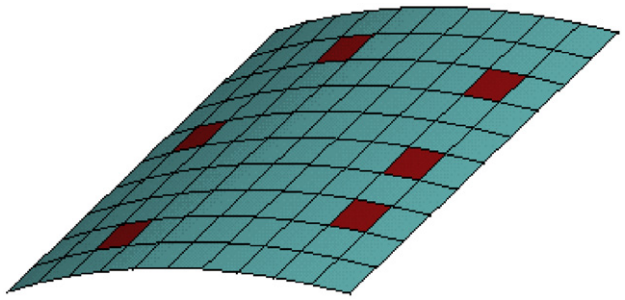

Fig. 18. Collocated sensors and actuators location on the cylindrical panel substrate based on maximum controllability index.

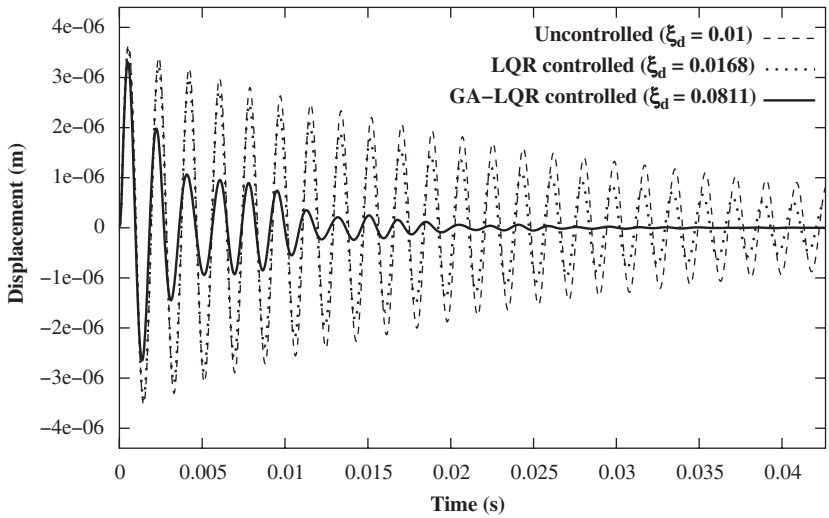

Fig. 19. Comparison of uncontrolled, LQR and GA-LQR controlled displacement history of the smart FRP composite cylindrical panel.

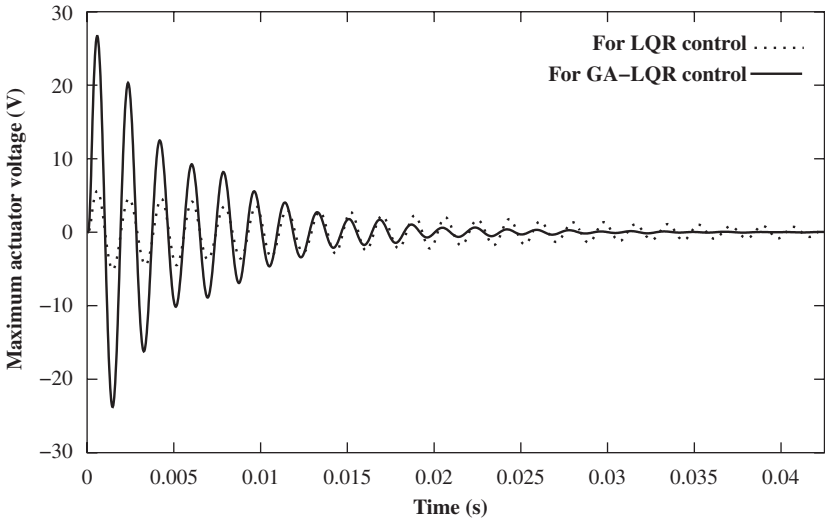

Fig. 20. Maximum actuator voltage variation for LQR and GA-LQR control scheme of cylindrical panel.

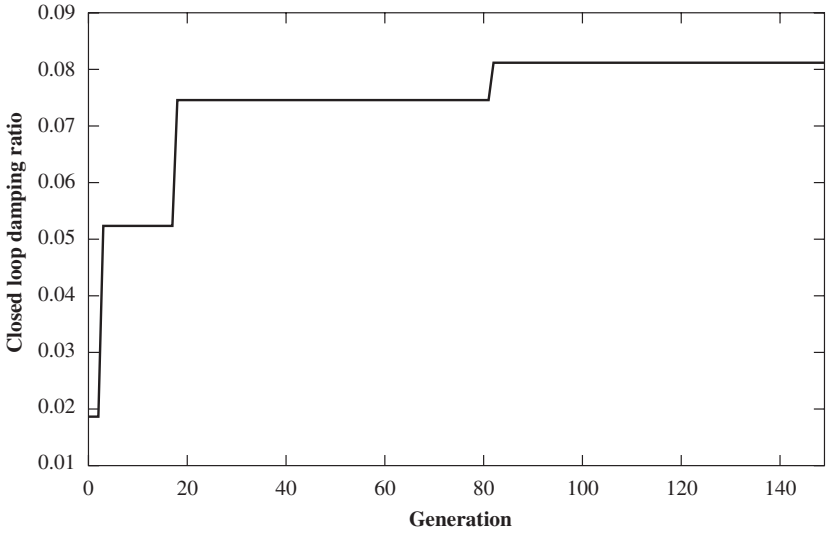

Fig. 21. Variation of closed-loop damping ratio with generation for cylindrical shell panel.

been determined using the following expressions:

$$[Q] = \begin{bmatrix} \alpha_2[\omega_i^2] & [0] \\ [0] & \alpha_1[I] \end{bmatrix} \quad \text{and} \quad [R] = \gamma[\hat{R}]$$

where ω_i^2 are the system eigenvalues and $[\hat{R}]$ is dielectric-coupling matrix of the actuators. First eight natural frequencies corresponding to different cases considered in the present work have been shown in Table 5. Table 6 shows the weighting parameters for optimal $[Q]$ and $[R]$ matrices for all the six cases considered in the present study along with the corresponding damping ratio, maximum input voltage, number of function evaluations required before convergence and CPU time. It could be observed from Table 6 that the effective damping ratio and input voltage have been significantly altered by energy weighting factors α_1, α_2 and γ. This also shows that the established fact that higher α_1 and α_1/α_2 lead to larger input voltage and higher

Table 5
List of first eight natural frequencies of the different models

Natural frequencies (kHz)	Spherical panel with		Cylindrical panel with Placement1
	Placement1	Placement2	
1st	8.454	8.592	0.3519
2nd	14.266	14.362	0.5458
3rd	17.126	17.473	0.6061
4th	17.365	17.831	0.7337
5th	21.366	21.436	0.7556
6th	24.129	24.501	0.7879
7th	26.263	26.524	0.9308
8th	31.830	32.006	0.9489

Table 6
List of energy weighting parameters for optimal [Q] and [R] matrices with CPU time and number of function evaluations for different models

Value of different parameters	Spherical with Placement1 using		Spherical with Placement2 using		Cylindrical Placement1 using	
	LQR	GA-LQR	LQR	GA-LQR	LQR	GA-LQR
α_1	26.400	87.218	17.500	0.7243	161.50	155.923
α_2	24.500	34.771	15.200	0.0375	120.70	70.431
γ	0.750	0.564	0.650	0.168	0.600	0.432
α_1/α_2	1.077	2.508	1.151	19.304	1.338	2.314
Closed-loop damping ratio (%)	1.18	12.03	1.0147	4.69	1.68	8.117
Maximum actuator voltage (V)	7.56	55.27	24.75	146.72	5.612	26.68
Converged CPU time (in s)	1.6	330.48	1.6	2838.24	1.5	1525.2
No. of functions evaluations	1	170	1	1460	1	820

damping ratio and change in γ has little effect on input voltage and effective damping ratio. It could be observed from Table 6 that the number of function evaluations is much higher in the case of GA-LQR scheme without optimal placement. The reason for the same is that in the absence of optimal placements most of the populations fail to satisfy the constraint of maximum input voltage. Therefore, even though GA-LQR chooses α_1, α_2 and γ such that input voltage is maximized but in the absence of optimal placement, actuation achieved is comparatively lower. It has also been observed from Table 6 that the CPU times consumed of LQR and GA-LQR for each function evaluation are more or less same.

8. Conclusions

In the present work an improved integer-coded GA-based combined optimal placement of PZTs patches and real-coded GA-based LQR control scheme has been developed for active vibration control of smart FRP composite shell structures. This combined module has been used in conjunction with the developed layered shell finite element procedure for coupled electromechanical analysis of smart shell structures. The present integer-coded GA-based optimal actuator location is especially advantageous for large structures where number of actuators is large. It has been observed that the proposed improved GA module leads to optimal locations of actuators. The improved GA-based LQR schemes show that the optimal placement obtained from the present method not only maximizes closed-loop damping ratio but also minimizes input voltages to the actuators. In the present method only three weighting factors have been used to search optimal [Q] and [R] matrices using improved real-coded GA, which reduces chromosome length and hence minimizes computational time. In fact, the computational time required for the present GA-based LQR scheme and

optimal actuator placement is almost same as that required for conventional LQR scheme. From the present study it could be observed that the combined GA-based placement and control scheme leads to a closed-loop damping ratio as high as 12% which is much higher compared to earlier reported results [9] while keeping the input voltages of the actuators within the limit.

References

[1] T. Bailey, J.E. Hubbard, Distributed piezoelectric polymer active vibration control of a cantilever beam, *Journal of Guidance, Control and Dynamics* 85 (1985) 605–611.

[2] E.F. Crawley, J. Luis, Use of piezoelectric actuators as elements of intelligent structures, *AIAA Journal* 25 (10) (1987) 1373–1385.

[3] C.K. Lee, Theory of laminated piezoelectric plates for the design of distributed sensors/actuators Part 1: governing equations and reciprocal relationships, *Journal of Acoustical Society of America* 87 (3) (1990) 1144–1158.

[4] H.S. Tzou, C.I. Tsang, Distributed piezoelectric sensor/actuator design for dynamic measurement/control of distributed parameter systems: a finite element approach, *Journal of Sound and Vibration* 138 (1) (1990) 17–34.

[5] S.H. Chen, G.F. Yao, C. Huang, A new intelligent thin shell element, *Journal of Smart Materials and Structures* 9 (2000) 10–18.

[6] K. Hiramoto, H. Doki, G. Obinata, Optimal sensor/actuator placement for active vibration control using explicit solution of algebraic Riccati equation, *Journal of Sound and Vibration* 229 (5) (2000) 1057–1075.

[7] Q. Wang, C. Wang, A controllability index for optimal design of piezoelectric actuators in vibration control of beam structures, *Journal of Sound and Vibration* 242 (3) (2001) 507–518.

[8] N. Zhang, I. Kirpitchenko, Modelling dynamics of a continuous structure with a piezoelectric sensor/actuator for passive structural control, *Journal of Sound and Vibration* 249 (2) (2002) 251–261.

[9] P. Bhattacharya, H. Suhail, P.K. Sinha, Finite element analysis and distributed control of laminated composite shells using LQR/IMSC approach, *Aerospace Science and Technology* 6 (2002) 273–281.

[10] D.A. Saravavanos, A.P. Christoforou, Impact response of adaptive piezoelectric laminated plates, *AIAA Journal* 40 (10) (2002) 2087–2095.

[11] K.K. Ang, S.Y. Wang, S.T. Quek, Weighted energy linear quadratic regulator vibration control of piezoelectric composite plates, *Journal of Smart Materials and Structures* 11 (2002) 98–106.

[12] S. Narayanan, V. Balamurugan, Finite element modeling of piezolaminated smart structures for active vibration control with distributed sensors and actuators, *Journal of Sound and Vibration* 262 (2003) 529–562.

[13] R.H. Christensen, I.F. Santos, Design of active controlled rotor-blade systems based on time-variant modal analysis, *Journal of Sound and Vibration* 280 (2005) 863–882.

[14] J.H. Han, L. Lee, Optimal placement of piezoelectric sensors and actuators for vibration control of a composite plate using genetic algorithms, *Journal of Smart Materials and Structures* 8 (1999) 257–267.

[15] A.M. Sadri, J.R. Wright, R. Wynne, Modeling and optimal placement of piezoelectric actuators in isotropic plates using genetic algorithm, *Journal of Smart Materials and Structures* 8 (1999) 490–498.

[16] M.M. Abdullah, A. Richardson, J. Hanif, Placement of sensors/actuators on civil structures using genetic algorithms, *Earthquake Engineering and Structural Dynamics* 30 (8) (2001) 1167–1184.

[17] I. Robandi, K. Nishimori, R. Nishimura, N. Ishihara, Optimal feedback control design using genetic algorithm in multimachine power system, *Electrical Power and Energy Systems* 23 (2001) 263–271.

[18] K. Deb, S. Gulati, Design of truss-structures for minimum weight using genetic algorithms, *Finite Elements in Analysis and Design* 37 (2001) 447–465.

[19] H.Y. Guo, L. Zhang, L.L. Zhang, J.X. Zhou, Optimal placement of sensors for structural health monitoring using improved genetic algorithm, *Journal of Smart Materials and Structures* 13 (2004) 528–534.

[20] Q.S. Li, D.K. Liu, J. Tang, N. Zhang, C.M. Tam, Combinatorial optimal design of number and positions of actuators in actively controlled structures using genetic algorithm, *Journal of Sound and Vibration* 270 (2004) 611–624.

[21] Y. Yang, Z. Jin, C.K. Soh, Integrated optimal design of vibration control system for smart beams using genetic algorithm, *Journal of Sound and Vibration* 282 (2005) 1293–1307.

[22] S.Y. Wang, K. Tai, S.T. Quek, Topology optimization of piezoelectric sensors/actuators for torsional vibration control of composite plates, *Journal of Smart Materials and Structures* 15 (2) (2006) 253–269.

[23] W. Liu, Z.K. Hou, M.A. Demetriou, A computational scheme for the optimal sensor/actuator placement of flexible structures using spatial H-2 measures, *Mechanical Systems and Signal Processing* 20 (4) (2006) 881–895.

[24] C. Swann, A. Chattopadhyay, Optimization of piezoelectric sensor location for delamination detection in composite laminates, *Engineering Optimization* 38 (5) (2006) 511–528.

[25] A.L. Buczak, H. Wang, H. Darabi, M.A. Jafari, Genetic algorithm convergence study for sensor network optimization, *Information Sciences* 133 (2001) 267–282.

[26] S.J. Habib, Modeling and simulating coverage in sensor network, *Computer Communications* 30 (2007) 1029–1035.

[27] Q. Wu, N.S.V. Rao, X. Du, S.S. Iyenger, V.K. Vaishnavi, On efficient deployment of sensors on planner grid, *Computer Communications* 30 (2007) 2712–2734.

[28] S. Hussain, A.W. Matin, O. Islam, Genetic algorithm for hierarchical wireless sensor network, *Journal of Networks* 2 (5) (2007) 87–97.

[29] S. Ahamad, B.M. Irons, O.C. Zienkiewicz, Analysis of thick and thin shell structure by curved elements, *International Journal of Numerical Methods in Engineering* 2 (1970) 419–451.
[30] F.L. Lewis, *Optimal Control*, Wiley, New York, 1986.
[31] J.C. Bruch, J.M. Sloss, I.S. Sadek, Optimal piezo-actuator locations/lengths and applied voltage for shape control of beams, *Journal of Smart Materials and Structures* 9 (2002) 205–211.
[32] K. Deb, S. Kartick, T. Okabe, Self-adaptive simulated binary crossover for real parameter optimization, *GECCO'07*, London, UK, 2007, pp. 1187–1194.
[33] J.N. Reddy, Exact solution of moderately thick laminated shells, *ASCE Journal of Engineering Mechanics* 110 (5) (1984) 794–809.
[34] W.S. Hwang, H.C. Park, Finite element modeling of piezoelectric sensors and actuators, *AIAA Journal* 31 (5) (1993) 930–937.
[35] H.S. Tzou, R. Ye, Analysis of piezoelectric structures with laminated piezoelectric triangle shell elements, *AIAA Journal* 34 (1996) 110–115.
[36] C.Y.K. Chee, L. Tong, G.P. Steven, A mixed model for composite beams with piezoelectric actuators and sensors, *Journal of Smart Materials and Structures* 8 (1999) 417–432.